

Evaluation and Real-Time Monitoring of Data Quality in Electrical Impedance Tomography

Yasin Mamatjan^{1,4}, Bartłomiej Grychtol², Pascal Gaggero³, Jörn Justiz³, Volker Koch³ and Andy Adler¹

¹ Systems and Computer Engineering, Carleton University, Ottawa, Canada

² German Cancer Research Center, Heidelberg, Germany

³ Bern University of Applied Sciences, Biel/Bienne, Switzerland

⁴ Electrical-Electronics Engineering, Zirve University, Turkey

Abstract—Electrical impedance tomography (EIT) is a non-invasive method to image conductivity distributions within a body. One promising application of EIT is to monitor ventilation in patients as a real-time bed-side tool. Thus it is essential that an EIT system reliably provide meaningful information, or alert clinicians when this is impossible. Because the reconstructed images are very sensitive to system instabilities (primarily from electrode connection variability and movement), EIT systems should continuously monitor and, if possible, correct for such errors. Motivated by this requirement, we describe a novel approach to quantitatively measure EIT data quality. Our goals are to: define the requirements of a data quality metric, develop a metric q which meets these requirements, and an efficient way to calculate it. The developed metric q was validated using data from saline tank experiments and a retrospective clinical study. Additionally, we show that q may be used to compare the performance of EIT systems using phantom measurements. Results suggest that the calculated metric reflects well the quality of reconstructed EIT images for both phantom and clinical data. The proposed measure can thus be used for real-time assessment of EIT data quality and, hence, to indicate the reliability of any derived physiological information.

Index Terms—Electrical impedance tomography, data quality, image quality, patient monitoring.

I. INTRODUCTION

Electrical impedance tomography (EIT) images the conductivity distribution within a body from current patterns and measurements made at electrodes attached to the body's surface. EIT imaging of the upper thorax is a promising tool for monitoring of lung ventilation to provide timely information on the state of lung tissue and identify regions of normal ventilation, lung collapse or overdistention [1], [2]. However, EIT measurements are subject to errors caused by human body dynamics (movement and sweat), electrode contact variability or loss, and electronic imperfections such as noise or drift. [3], [4]. If treated as valid signal, the potentially large number of false alarms caused by such errors can render the device useless in the clinical environment. It is therefore necessary for an EIT system to recognize and compensate for such errors, or alert clinicians when this is not possible, rather than quietly presenting inaccurate information. There is therefore a need for a reliable data quality indicator to continuously assess the acquired data in real-time and ensure that diagnostic or therapeutic decisions are based on accurate information.

Overall, data quality is an increasingly salient topic in biomedical engineering. As biomedical data acquisition and

processing systems support (or take) more decisions in modern societies, from the clinic to border control, accurate data becomes of paramount importance. Poor quality data can lead to wrong decisions with grave consequences. In the field of biometrics, for instance, dedicated workshops have already been conducted [5] and a systematic taxonomy (character, fidelity and utility) for image quality has been developed [6]. Systematic approaches to data quality assessment have been proposed (e.g., [7]). Several studies tackled the issue of signal quality in electroencephalography (EEG) (e.g., [8], [9]) which, like EIT, uses voltage readings from multiple electrodes on the body's surface. However, to the best of our knowledge, no systematic approach to measures of data quality suitable for real time monitoring have been derived.

While EEG signals from individual electrodes are generally analyzed independently, EIT imaging depends on data from all electrodes for image reconstruction. Additionally, in most practical systems, data from different electrodes are interdependent to a degree. A single measurement error can cause the failure of image reconstruction. Thus, past effort has been directed at detecting and compensating for these errors. Asfaw and Adler [10], [11] proposed a method of automatic detection of faulty electrodes and unreliable measurements by means of finding single electrodes whose readings are inconsistent with the rest, an idea which we further exploit here. Boverman et al. [12] described the use of the complete electrode model (CEM) to compensate for badly connected electrodes. They suggested to take into account during the reconstruction the actual electrode contact impedance, for which analytical solutions exist [13], albeit only for a 2D homogeneous disk, and a fast statistical estimation method using Magic Toeplitz Matrix have been developed [14]. However, these methods are not suitable for continuous monitoring because of the unstable procedure for the failing electrodes and the need for recalculating the sensitivity matrix for the changes of CEM parameters. An online algorithm for the management of faulty electrodes based on the principle of reciprocity for EIT measurements was developed by Hartinger et al. [15]. However, in ventilation, imaging reciprocity is broken by physiological changes occurring between measurements, particularly for slower EIT systems or during high-frequency ventilation. More practical and fast-processing approaches are needed for real-time monitoring applications.

Development of signal quality measures has also been

motivated by the desire to assess and compare the performance of EIT systems. Although signal to noise ratio (SNR) is commonly used, its value may vary greatly according to test conditions and capacity of the testing system and depends on the number, location, and distribution of the electrodes [16]. Thus it is difficult to compare different EIT systems in terms of SNR. Riu and Anton [17] proposed an additional measure to assess the quality of EIT measurements based on comparing the actual and expected signals from a known test object. A procedure and a set of parameters to evaluate and calibrate the performance of EIT using a saline phantom and cubic test objects was also proposed [18]. These approaches are not suited for online data quality monitoring in ventilation imaging where no test object can be placed inside the body.

Another approach is to assess the quality of the reconstructed images rather than the signal used to calculate them. A comprehensive set of parameters for assessment of EIT reconstruction algorithms in terms of image quality has been proposed [19]. While EIT image quality naturally depends on data quality, the reconstructed images are also strongly dependent on the reconstruction strategy and in particular the choice of the regularization (hyper)parameter. Furthermore, noise is likely to be amplified through the reconstruction process [20] due to meshing errors, resulting in image artifacts and degraded image quality, while a single (partially) disconnected electrode can cause complete failure of image reconstruction despite good data from all other electrodes. Thus, an image-based quality metric is not well suited for unsupervised real-time assessment of data quality.

In order to address the requirement for continuous EIT data quality assessment for monitoring applications in the intensive care unit (ICU), a novel formulation to measure data quality is proposed. Our goal is to provide a quantitative assessment of data quality suitable for real-time display alongside the reconstructed images and hence able to affect clinical decisions.

The paper is organized as follows: In the next section, we first state the requirements for a useful data quality metric. We then elaborate our formulation of such a metric (II-B), and describe the data and procedure used to evaluate it. After presenting the results in section III, we discuss the proposed quality metric in terms of the identified requirements and offer concluding remarks in section IV.

II. METHODOLOGY

In this section we first present the requirements a data quality measure q for EIT should satisfy and a short overview of our approach to derive such q . Second, we elaborate the formulation of q . Lastly, we describe the data and procedures used for its evaluation.

A. Overview

In order for a data quality metric q to be easily interpretable and able to inform diagnostic interpretation of EIT images, it should satisfy the following requirements:

- 1) q should vary between 0 and 1 ($0 \leq q \leq 1$) such that q of 1 (a high value) indicates a good signal, while 0 (a low value) stands for a bad signal.

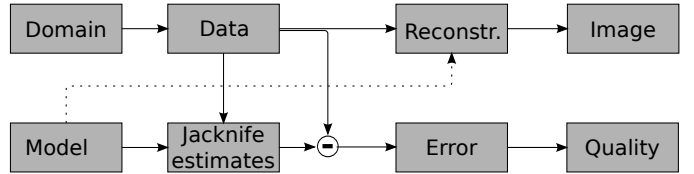


Fig. 1: A graph showing the general overview for data quality calculation based on a model and data.

- 2) q should *increase* as we include more data (q from $E+1$ good electrodes $>$ q from E good electrodes).
- 3) q should *decrease* as we include bad data (q from E good electrodes + 1 bad electrode $<$ q from E good electrodes).
- 4) q should *decrease* if data are good but incorrect (e.g. electrodes were placed incorrectly).

It is clear that in order to satisfy the last requirement the quality metric q must take into account a model of the studied domain and the specific measurement strategy employed (forward model). We thus base our approach to measure data quality on the jackknife concept [21]. In short, based on a forward model and a vector of voltage differences, we attempt to recover the value of each individual measurement from all the other measurements (the jackknife estimate). By comparing the actual measurements with their estimates, we calculate measurement errors which we scale, transform and aggregate into a single scalar quantity with the desired properties. Our approach is illustrated schematically in Fig. 1.

B. Data quality formulation

We consider the large class of linear EIT reconstruction algorithms based on the sensitivity matrix approach. We formulate q for normalized difference reconstruction, which is a common approach in thoracic EIT due to its increased resilience to movement and shape errors with respect to the (not normalized) difference approach. However, the formulation for difference imaging is equivalent, differing only by a scale factor.

During an EIT measurement, we acquire normalized voltage difference data $\mathbf{d} = (\mathbf{v} - \mathbf{v}_r) / \mathbf{v}_r$, where \mathbf{v} and \mathbf{v}_r are the current and reference measurements, respectively. From \mathbf{d} we wish to reconstruct images of relative conductivity changes $\mathbf{m} = (\boldsymbol{\sigma} - \boldsymbol{\sigma}_r) / \boldsymbol{\sigma}_r$ between two states: the current conductivity distribution $\boldsymbol{\sigma}$ and the reference conductivity distribution $\boldsymbol{\sigma}_r$ inside the medium. Such difference, or functional, imaging is well suited for, e.g., monitoring of physiological changes during breathing.

The data \mathbf{d} and image \mathbf{m} are related by a physics model $F(\cdot)$:

$$\mathbf{d} = F(\mathbf{m}) \approx \mathbf{J}\mathbf{m} \quad (1)$$

where \mathbf{J} is the $M \times N$ sensitivity (or Jacobian) matrix which linearizes the model $F(\cdot)$ at a background (or reference) conductivity $\boldsymbol{\sigma}_r$, M is the data length, and N is the number of elements in the image \mathbf{m} . \mathbf{J} is calculated as:

$$[\mathbf{J}]_{i,j} = \frac{\partial [F(\boldsymbol{\sigma}_r)]_i}{\partial [\boldsymbol{\sigma}_r]_j} \quad (2)$$

for $i = 1 \dots M$ and $j = 1 \dots N$. \mathbf{J} is often calculated by the finite element method (FEM) and depends on (a model of) the medium's shape and background conductivity distribution as well as electrode placement and measurement strategy.

We wish to define the vector $\varepsilon \in \mathbb{R}^M$ — the error to signal ratio — as the estimated error over signal, such that for $i = 1 \dots M$

$$\varepsilon_i = \frac{d_i - \hat{d}_i}{S} = \frac{1}{S} \left(\boldsymbol{\theta}_i^T (\mathbf{d} - \hat{\mathbf{d}}_i) \right), \quad (3)$$

where $\mathbf{d} \in \mathbb{R}^M$ is the vector of measured data, and $\hat{\mathbf{d}}_i$ is a jackknife estimate of \mathbf{d} based on all the data \mathbf{d} but its i -th element, $\boldsymbol{\theta}_i$ is a vector ($M \times 1$) of zeros with a single element $[\boldsymbol{\theta}_i]_i = 1$ and S represents signal strength. However, we do not know *a priori* what constitutes the “signal” in an EIT measurement. Instead, we define S as the mean of normalized difference data obtained by simulating using Eq. 1 the appearance of a small (20% medium radius) spherical contrast (2:1 contrast-to-background conductivity ratio) at the center of the medium.¹

The first order jackknife estimate, $\hat{\mathbf{d}}_i$, is obtained by reconstructing an image $\hat{\mathbf{m}}_i$ using all data \mathbf{d} except its i -th element

$$\hat{\mathbf{m}}_i = \mathbf{R}_i \mathbf{d}, \quad (4)$$

and then projecting the data from this estimate

$$\hat{\mathbf{d}}_i = \mathbf{J} \hat{\mathbf{m}}_i = \mathbf{J} \mathbf{R}_i \mathbf{d}, \quad (5)$$

where \mathbf{R}_i is the reconstruction matrix that can be written in the *Wiener filter form* [20] as:

$$\mathbf{R}_i = \boldsymbol{\Sigma}_m \mathbf{J}^T (\mathbf{J} \boldsymbol{\Sigma}_m \mathbf{J}^T + \lambda^2 \boldsymbol{\Sigma}_n)^{-1} \quad (6)$$

where $\boldsymbol{\Sigma}_m$ is an estimate of the prior model element covariance, while $\boldsymbol{\Sigma}_n$ is an estimate of the data noise covariance, and λ is a hyperparameter controlling the amount of regularization. The required amount of regularization depends on the forward model from which \mathbf{J} and $\boldsymbol{\Sigma}_m$ are derived. To cater for any model, here λ is set objectively such that noise amplification as defined in [20] in the center of the medium equals 1. This configuration-independent method of setting the hyperparameter has been shown to consistently produce good quality reconstructions qualitatively indistinguishable from expert heuristic selection and with close to optimal resolution [22].

Typically, we assume that all data noise is equal on each channel and thus $\boldsymbol{\Sigma}_n = \mathbf{I}$. However, the reconstruction matrix \mathbf{R}_i explicitly ignores data channel i , and thus assumes that data noise on channel i is *much* larger (by an additive factor $\mu \gg 0$), which we model as

$$\mathbf{R}_i = \boldsymbol{\Sigma}_m \mathbf{J}^T (\mathbf{J} \boldsymbol{\Sigma}_m \mathbf{J}^T + \lambda^2 (\mathbf{I} + \mu \boldsymbol{\Theta}_i))^{-1} \quad (7)$$

where $\boldsymbol{\Theta}_i$ is a matrix ($M \times M$) of zeros with $[\boldsymbol{\Theta}_i]_{ii} = 1$ [23]. Thus, we have

$$\begin{aligned} \varepsilon_i &= \frac{1}{S} \left(\boldsymbol{\theta}_i^T (\mathbf{d} - \hat{\mathbf{d}}_i) \right) = \frac{1}{S} \left(\boldsymbol{\theta}_i^T (\mathbf{d} - \mathbf{J} \mathbf{R}_i \mathbf{d}) \right) \\ &= \frac{1}{S} \left(\boldsymbol{\theta}_i^T (\mathbf{I} - \mathbf{J} \mathbf{R}_i) \mathbf{d} \right). \end{aligned} \quad (8)$$

¹Here, for difference imaging, we would use kS instead of S , where k is a scaling factor accounting for the possibly different scales of the simulated and real signal (due to signal amplification/attenuation or modeling inaccuracies in \mathbf{J}).

We define a “quality” matrix, \mathbf{Q} which represents this calculation for each data element. Each row i of \mathbf{Q} is given by $\mathbf{Q}_i = \boldsymbol{\theta}_i^T (\mathbf{I} - \mathbf{J} \mathbf{R}_i)$. \mathbf{Q} can be precalculated, as it depends only on the geometry, and the stimulation and measurement patterns. Thus

$$\varepsilon = \frac{1}{S} (\mathbf{Q} \mathbf{d}) \quad (9)$$

\mathbf{Q} can be calculated efficiently, as shown in Appendix A, the code for which will be part of the next release of the EIDORS suite [24].

Finally, to derive the proposed quality measure q , we first calculate a vector \mathbf{q} expressing the quality of each measurement i as

$$q_i = \left(\frac{1}{2} \right)^{|\varepsilon_i|}. \quad (10)$$

Thus, $\lim_{|\varepsilon_i| \rightarrow 0} q_i = 1$ indicating perfect quality, and $\lim_{|\varepsilon_i| \rightarrow \infty} q_i = 0$ for bad quality data. While any positive number < 1 would satisfy the requirements of our formulation, our choice means that when $|\varepsilon_i| = 1$, $q_i = \frac{1}{2}$, which we feel helps interpretation of the calculated values.

The proposed data quality measure q is the arithmetic mean of all the elements of \mathbf{q}

$$q = \frac{1}{M} \sum_{i=1}^M q_i, \quad (11)$$

where M is the length of the data vector \mathbf{d} . The calculation of q requires one matrix multiplication per data set (eq. 9), which is comparable to the computational requirement of linear image reconstruction.

C. Evaluation

The proposed quality metric q was evaluated under laboratory and clinical conditions. We used a physical phantom to investigate several scenarios where a variable number of electrodes were affected by degraded contact quality. Recordings from two pediatric patients with lung disease from a published study were utilized to assess performance and demonstrate the utility of q in the clinical setting. We evaluated q in light of the requirements identified in section II-A and by comparison with bespoke measures of image quality. Additionally, although not the main focus of this study, we used q to compare the performance of three available EIT systems using phantom measurements.

1) Data:

a) *Phantom measurements:* The phantom test system consisted of a cylindrical plastic tank filled with saline solution, a cubic test target and the Sigma Tome II EIT system (Ecole Polytechnique Montréal, Canada). The tank (diameter = 29 cm, height = 36 cm) was filled with 22 liters of saline solution (conductivity $\sigma = 0.8 \text{ Sm}^{-1}$ as measured with a conductivity meter ECTestr (Oakton Instruments, USA)) and equipped with 4 rows of 32 electrodes of which 16 equidistant electrodes on a single row approximately 17 cm below the water surface were used.

Different degrees of electrode contact deterioration were obtained through varying the contact resistance of individual

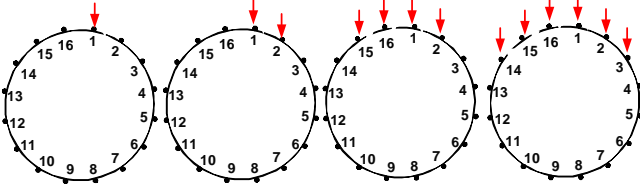


Fig. 2: Test scenarios with 1, 2, 4 and 6 affected electrodes.

electrodes by either connecting a resistor between the electrode and the connector on the tank, or completely disconnecting the electrode. The resistor values used were 0 (no additional resistor), 1 k Ω , 4.7 k Ω , 100 k Ω and open circuit. Measurements with 0, 1, 2, 4 and 6 affected electrodes were collected. As shown in Fig. 2, we considered a typical pattern of failure for belt-mounted electrodes whereby multiple neighboring electrodes become simultaneously disconnected. This also represents the worst-case scenario in terms of sensitivity loss.

For each resistor value and number of affected electrodes, first a homogeneous measurement was acquired to be used as reference for difference imaging the subsequent acquisitions with a non-conductive ($\sigma \ll 10^{-4}$ Sm $^{-1}$) plastic cube of 100 ml (4.6 cm side length) as a target. The target was suspended at the level of the electrode plane from a robotic arm placed above the tank [18]. It was moved across the tank along a line passing through its center in 7 steps of 4 cm. The system was allowed to rest for at least 15 seconds after moving the target to the next position before the next measurement was acquired in order for the water surface to stabilize.

A typical 16-electrode EIT system with adjacent stimulation and voltage measurement patterns was used. Current was injected between a pair of adjacent electrodes and voltages were measured between all other pairs of adjacent electrodes (13 in total). Thus, for each data frame, 208 (16×13) voltage measurements were acquired of which only 104 are independent due to reciprocity. All measurements were taken under normal room temperature of 20°C.

b) Clinical data: The human breathing data were taken from [25]², where pediatric patients with acute lung injury or acute respiratory distress syndrome (ALI/ARDS) were recruited to monitor their lung mechanics during mechanical ventilation using EIT. The experimental protocol consisted of (i) a baseline ventilation stage, (ii) a lung recruitment stage, and (iii) a PEEP (positive end-expiratory pressure) titration stage with sequentially decreased airway pressure. A tidal volume of 6 mL/kg of body weight was used as baseline ventilation using volume-controlled (VC) mode. During the lung ventilation stage, patients were ventilated in pressure-controlled (PC) mode with sequentially increased airway pressure. During the PEEP titration stage, PEEP level was decreased sequentially to the lowest possible setting.

Measurements were acquired using the Goe-MT II EIT device (CareFusion, Hoechberg, Germany) operated in single

frequency, where 16 electrodes were used, and adjacent stimulation and measurement patterns were applied. Here we use the measurement data of patient 1 and 7 from the original study [25], where further details can be found. Patient 1 is representative of the study; images at all stages of the protocol grossly correspond to expectations (shift of ventilation to lower parts of the image at higher PEEP). Reconstructions for patient 7 are physiologically implausible for at least two stages of the protocol and have more artifacts, despite best attempts (thorax-shape model, motion compensation, Gaussian smoothing filter).

c) System evaluation: Three available EIT systems were used to acquired measurements on the phantom described above. A smaller cubic plastic target (volume 50 ml, side length 3.6 cm) was suspended in the saline solution at the level of the electrode plane and moved from the center of the tank outwards in 7 steps of 2 cm. A total of 20 data frames acquired by each system were analyzed. To avoid unfair comparison, the results are reported as originating from System A, System B or System C, without referring to any specific system or manufacturer.

2) Data processing: All analysis and data processing reported here were carried out in MATLAB (The Mathworks, Natick, MA) using EIDORS 3.6³ [24]. EIT reconstructions of phantom data were calculated using the one step Gauss-Newton solver with a Laplace spatial prior and assuming equal noise on each normalized difference data channel. To demonstrate that the remaining electrodes still provide good data, and thus validate our experimental design, we also reconstructed the phantom data using the strategy of [23], which removes the influence of specific measurements without introducing artifacts caused by replacing them with zeros. For reference, we also calculated the q metric for the hypothetical situation where less measurements were acquired (we removed measurements originated from the affected electrode(s) from the data vector \mathbf{d} and, consequently, from the Jacobian matrix \mathbf{J}). We used the ‘d2c2’ 2D FEM models from EIDORS’ `mk_common_model` function for calculating the Jacobian \mathbf{J} and reconstructing the phantom data. For clinical data we tried the thorax-shaped ‘d2t2’ 2D model as well as the ‘adult_male_16el_lungs’ 3D FEM provided by the `mk_library_model` function in our attempts to obtain good reconstructions of the suspect data.

To assess the proposed data quality metric q , we devised two ad hoc measures of image distortion caused by deteriorated electrode contact to compare against. We used the fact that in our controlled experiment we know what the reconstructions look like when all electrodes are properly connected (the “reference” image) and how they deteriorate as electrodes become disconnected. Since they require knowledge of the expected result, these ad hoc measures are not possible surrogates for the proposed data quality. The measures are:

- **Deviation from reference image (D)** calculated as the average absolute value of element-wise difference between a given image $\hat{\mathbf{m}}$ and a reference image $\hat{\mathbf{m}}_{\text{ref}}$, normalized to mean absolute element value in the refer-

²available at http://eidors3d.sourceforge.net/data_contrib/cg-2012-ards-recruitment/cg_2012_ards_recruitment.shtml

³<http://www.eidors.org>

ence image:

$$D(\hat{\mathbf{m}}) = \frac{|\overline{\hat{\mathbf{m}}} - \hat{\mathbf{m}}_{\text{ref}}|}{|\hat{\mathbf{m}}_{\text{ref}}|} \quad (12)$$

where $\overline{(\cdot)}$ denotes the arithmetic mean of all the vector's values and $|\cdot|$ the per-element absolute value.

- **Image standard deviation (S)** calculated from all values in a reconstructed image $\hat{\mathbf{m}}$. This measure is motivated by our observation that reconstructions of tank measurements with all electrodes properly connected are smooth, whereas deteriorated electrode contact results in high amplitude ripples (c.f. Fig. 3a)

$$S(\hat{\mathbf{m}}) = \sqrt{\frac{1}{M} \sum_{i=1}^M (\hat{m}_i - \overline{\hat{\mathbf{m}}})^2}. \quad (13)$$

III. RESULTS

A. Phantom Measurements

Sample reconstructions from the phantom study are presented in Fig. 3a. Superimposed on the documented [26] features of one step Gauss-Newton solvers (which are characterized by increased ringing close to the boundary and loss of amplitude in the center of the medium) a clear pattern emerges, whereby the more electrodes fail the more artifacts appear in the image, particularly in the vicinity of the affected side (top). For comparison, in Fig. 3b we show reconstructions of the same data after accounting for the affected electrodes using the approach of [23]. Image artifacts are considerably reduced, but targets close to the affected side are not reconstructed correctly, as a result of the aforementioned loss of sensitivity.

Fig. 4 shows the relationship between the proposed quality metric q and the target position for the different numbers of affected electrodes and two resistor values. Overall, signal quality q fell as more electrodes were affected. In benign cases (up to 1 affected electrode), q was uniform across the bulk of the medium, falling off slightly close to the boundary. However, as more electrodes were affected on one side of the phantom, q began to exhibit position dependence, although no clear pattern emerged.

Values of q averaged over all target positions for different resistor values are reported in Fig. 5 as a function of the number of affected electrodes. For reference, the q values obtained by removing the affected measurements from the data vector \mathbf{d} and the Jacobian \mathbf{J} are also shown (indicated as "rmvd"). The average quality q deteriorates as electrodes fail, with higher resistor values causing greater decrease. Measurements recorded with the 1 k Ω resistor show only very slight decrease in quality. This is also reflected in the images reconstructed from these measurements which do not show noticeable artifacts until 4 electrodes fail, and even then only close to the affected side (images not presented). The quality obtained when ignoring all affected data is always higher than that containing more, but corrupt, data. Interestingly, excluding the first electrode resulted in a slight increase in q .

Finally, Fig. 6 presents the relationship between the data quality q and the ad hoc measures of image distortion D and

S introduced in section II-C2. A clear relationship is observed on both graphs. q is very sensitive to both D and S ; it falls rapidly as either metric increases (hence the logarithmic scale on the graphs).

B. Clinical data

The average data quality values for the two patients at each stage of the protocol in [25] (described in section II-C1b), are shown in Fig. 7, along with our reconstructions with different reconstruction algorithms. Data from patient 1 exhibits consistent, high q values; its reconstructions show the expected shift of ventilation to dorsal (dependent) lung areas (lower part of the image) as PEEP is increased (R1–R4) and respective ventral movement during the downward PEEP titration (T1–T4). In contrast, q values for data from patient 7 are lower and reconstructions show more artifacts. Data quality is particularly low at stages R3 and T1; this is corroborated by worst, physiologically implausible or outright failed, reconstructions at these stages.

Analysis of the standard deviation of difference data (not presented) revealed 3 times higher noise at these stages as compared to the other protocol steps. This could be caused by patient movement or partial electrode disconnection.

C. System evaluation

The q values together with reconstructed images for the three evaluated EIT systems A, B, and C are presented in Fig. 8. System A showed stable high data quality values, with a slight tendency to decrease as the target was moved closer to the boundary. Data recorded by System B were of the lowest quality in the central part of the medium, but show comparatively little position dependence. The quality of data provided by System C was most sensitive to target position. The data quality values in Fig. 8a are consistent with the visual appearance of the reconstructed images in Fig. 8b (all of which were reconstructed with the Gauss-Newton algorithm introduced in section II-C2): System A and B show, respectively, least and most artifacts throughout, while for system C artifacts are weak when the target is in the center and strong close to the boundary. These results also reflect findings of an earlier study comparing the three systems [18], where it was found that systems B and C exhibit higher per-channel errors than system A.

IV. DISCUSSION AND CONCLUSION

In this paper, we proposed a novel approach to assess data quality of an EIT system quantitatively and evaluated its performance in laboratory and clinical conditions, as well as a means of assessing EIT system performance. In section II-A, we set out with a list of requirements that a useful quality metric should possess. We discuss them in light of the presented results as follows:

- 1) q should vary between 0 and 1: this is guaranteed by eq. 10 and 11. However, more work is required to determine the threshold q below which the data is no longer usable, and our experience with three different

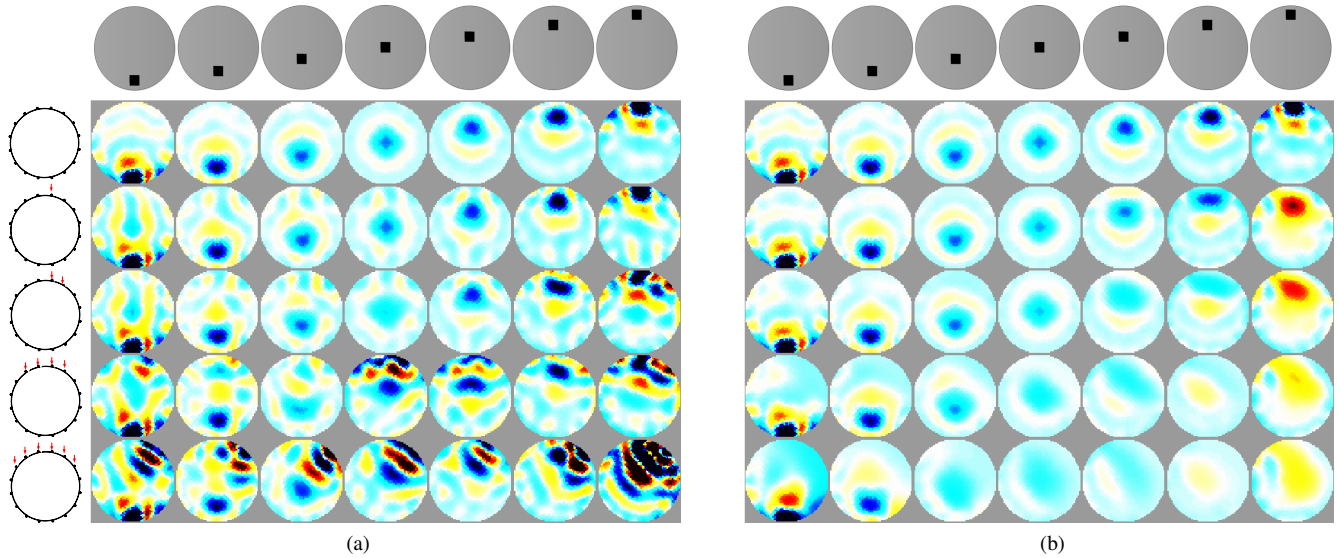


Fig. 3: (a) Reconstructions of phantom measurements of several target positions (indicated on top) obtained with different numbers of affected electrodes (indicated on the left). Contact quality of the indicated electrodes was degraded by the introduction of a 4.7 k Ω resistor. (b) Reconstructions of the same data using the approach of [23] which reduces the impact of data from the affected electrodes.

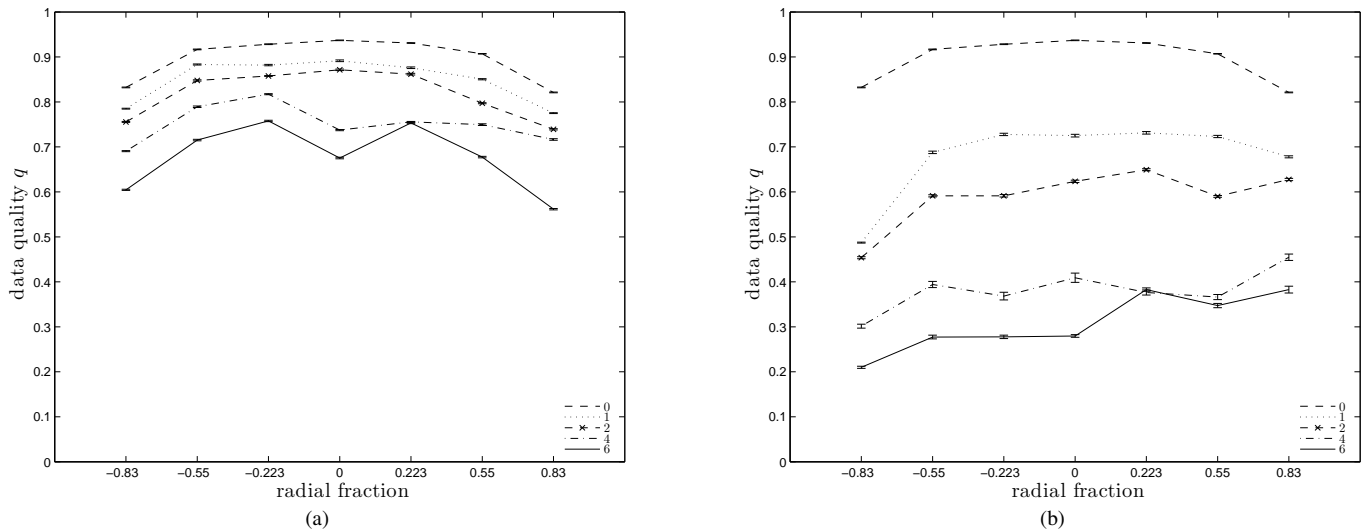


Fig. 4: Graphs showing the relationship between q values and target position for various numbers of affected electrodes (indicated in the legends) and resistor values of (a) 4.7 k Ω and (b) 100 k Ω . Higher values on the horizontal axis indicate greater proximity to the location of the affected electrodes (c.f. top diagrams in Fig. 3). Error bars indicate standard errors from 20 measurements.

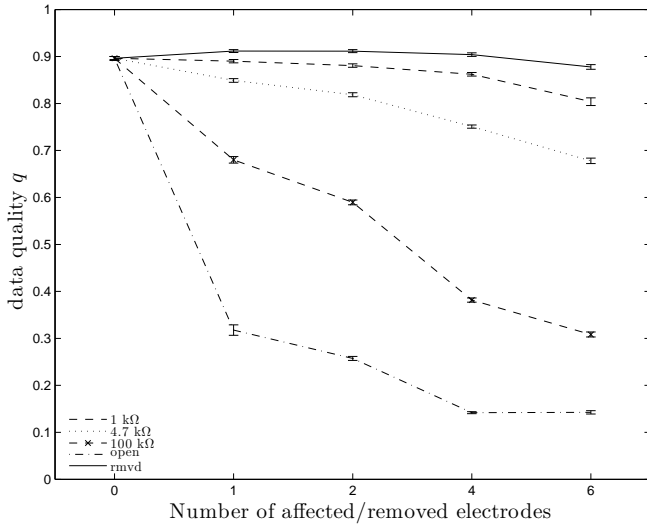


Fig. 5: Average data quality q as a function of the number of affected electrodes. Electrodes were either disconnected (“open”), removed from the recorded data (“rmvd”), or had their contact quality deteriorated by the introduction of resistors with the specified values. Each point represents an average value of 140 measurements (20 measurements for each of the 7 target positions). Error bars express standard error.

EIT systems suggests that such a threshold may be system-specific.

- 2) q should increase as we include more good data: although this feature is not mathematically guaranteed in our formulation, it is implicitly embedded in our method through its reliance on the jackknife estimates whose accuracy will increase as more good electrodes are added onto the medium. However, this increase is subject to the law of diminishing returns, conditional on the quality of the additional data, and depends on the positioning of the electrodes on the body surface. This is exemplified by the slight increase in q we observed in Fig. 6 after measurements associated with the first electrode were removed from the data vector \mathbf{d} ; further analysis revealed that measurements from electrode 1 happened to have the lowest average quality in our experiment. Nonetheless, the downward trend in q with reduced data is evident in Fig. 6.
- 3) q should decrease as we include bad data: this requirement is satisfied as evidenced by Fig. 6, where q is lower in all instances when electrodes affected by low quality contact are included in the data as compared to when they are excluded.
- 4) q should decrease if data are good but incorrect: although we did not present results to demonstrate this feature of q , it can be intuitively argued that when the acquired data do not correspond to the model (specifically, the Jacobian \mathbf{J}) used to calculate the jackknife estimates, the latter will be a poor fit for the data so q will be low. A mismatch between model and data occurs not only when electrodes are placed incorrectly, but

also when assumptions about the shape and conductivity distribution of an imaged body are inaccurate.

Another desirable property of a quality metric is consistency with respect to the type of data error, meaning that data affected by equivalent errors should be marked with the same quality score. However, because the impact of an electrode error in EIT depends on a multitude of factors such as the electrode’s position, the imaged body’s conductivity distribution, the location of conductivity changes within it, the stimulation and measurement strategy as well as the performance of the other electrodes and the characteristics of the EIT system, it is unclear how equivalent errors can meaningfully be defined for EIT. Thus, we did not include this property among the requirements for q .

In all our analyses, q was found to correspond well with the subjective and, in the case of the phantom study, objectively quantified image quality. Whenever q was lower, artifacts appeared on the images. This is particularly evident from the comparison of q with the ad hoc image distortion metrics presented in Fig. 6 (which are only possible to calculate because in the controlled environment of a phantom model we know what the images are supposed to look like). However, because q is independent of the user’s reconstruction algorithm, it is not causally related to the appearance of artifacts. Indeed, some of our reconstructions of the clinical measurements found to be suffering from low data quality (Fig. 7) appeared sufficiently plausible that they could be mistaken for valid images and analyzed. An indicator based on the quality metric we propose would allow doctors to better assess the plausibility of images and thus prevent erroneous diagnosis.

Also in comparing the three available EIT systems q offered useful quantitative information that was not otherwise apparent. All three systems had very similar average SNR values of 44.2, 44.5 and 45.9 dB for systems A, B and C, respectively. This result lends further support to the claim that SNR is a poor indicator of EIT system performance.

Encouragingly, our analysis of the impact of severity of electrode contact deterioration presented in Fig. 5 revealed that small variations in contact impedance (here, a 1 kΩ resistor) have only very slight impact on data quality. Because such small changes in skin contact are an inevitable consequence of human physiology, this result is particularly reassuring for the application of EIT as a long-term ventilation monitoring tool.

Because we set out to develop a data quality metric, as opposed to an image quality indicator, we explicitly formulated q to be independent of whatever reconstruction algorithm is used to reconstruct the data (but not the model of the domain from which they originate, i.e. the Jacobian matrix). This we achieved by embedding a fixed way to derive a reconstruction matrix into the calculation of the jackknife estimates on which our metric is based (eq. 6). It is conceivable, however, that the same reconstruction algorithm used to reconstruct the EIT images could inform the jackknife estimates. Thus, q would reflect not only the quality of the acquired data, but also the faithfulness of the reconstructions to the data.

Our purposeful design of the quality metric to be dependent on the model of the domain, in order to allow detecting data

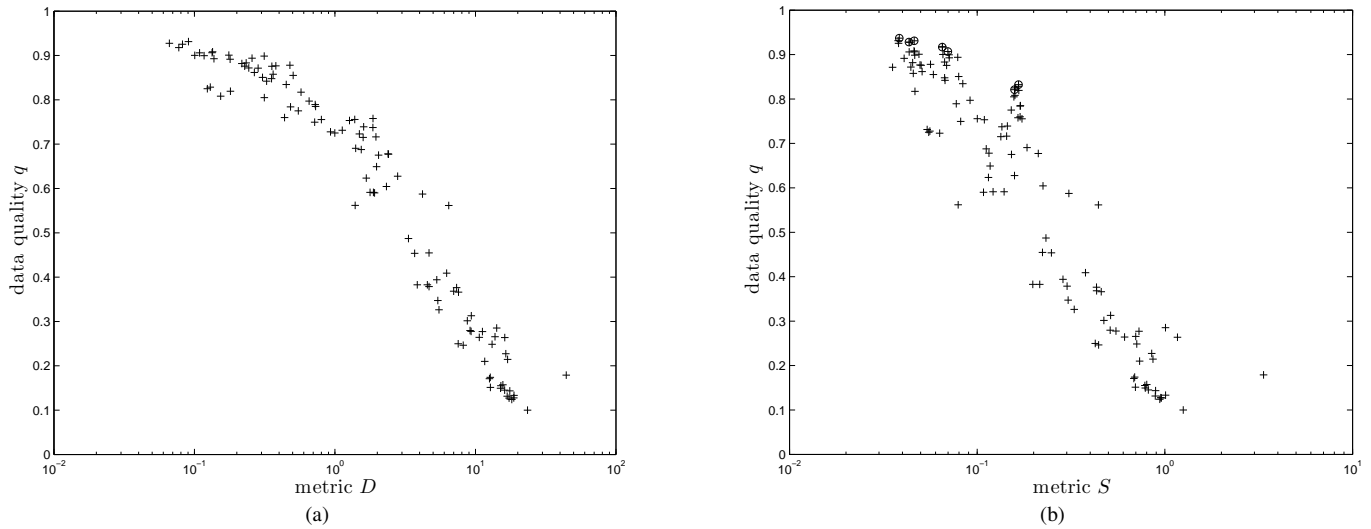


Fig. 6: Graphs showing the relationship between q values and the ad hoc image quality metrics (a) D and (b) S (see section II-C2). Each point represents an average of 20 measurements for each applicable combination of resistor value and number of affected electrodes. Points corresponding to reference measurements (i.e. all electrodes, no resistors) are additionally marked with circles. Note the logarithmic scaling of the horizontal axes.

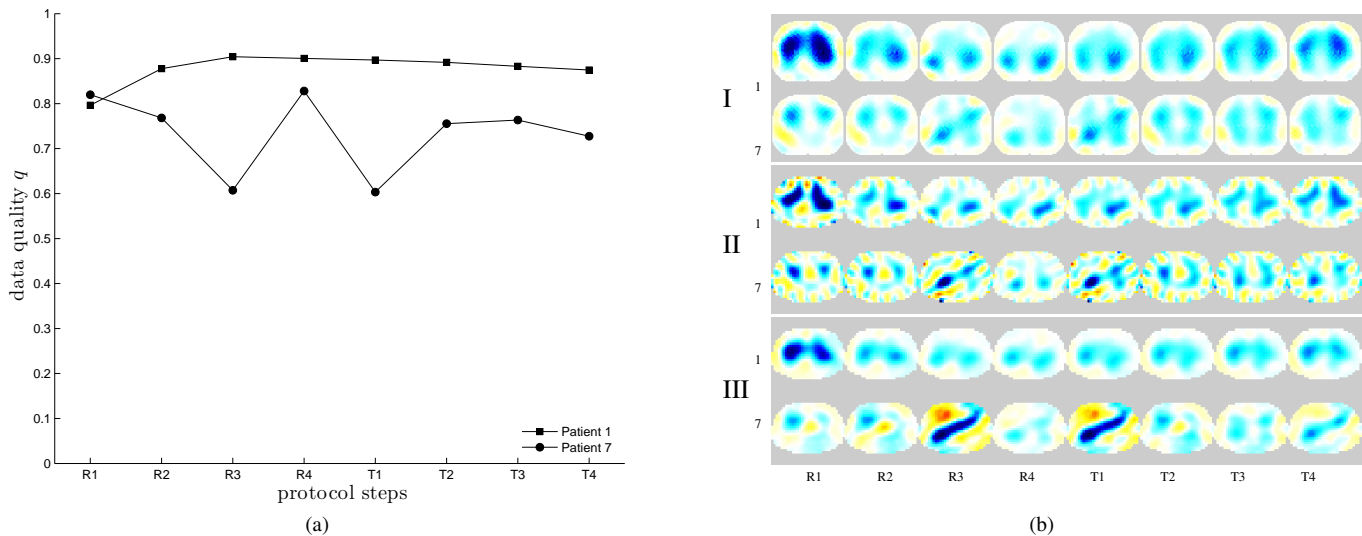


Fig. 7: Clinical data (patients 1 and 7 from [25]): (a) data quality metric for each stage of the protocol for both patients; and (b) the corresponding reconstructions obtained with I: one-step Gauss-Newton solver with Gaussian high pass filter image prior and movement compensation [27] and a 2D forward model, II: one-step Gauss-Newton solver with Laplace image prior and a 3D forward model, and III: GREIT algorithm built on a forward model including lung tissue contrast based on a CT from an adult male (not part of the study) [26]. Protocol: R1–R4 — recruitment by increasing PEEP; T1–T4 — PEEP titration (decrease).

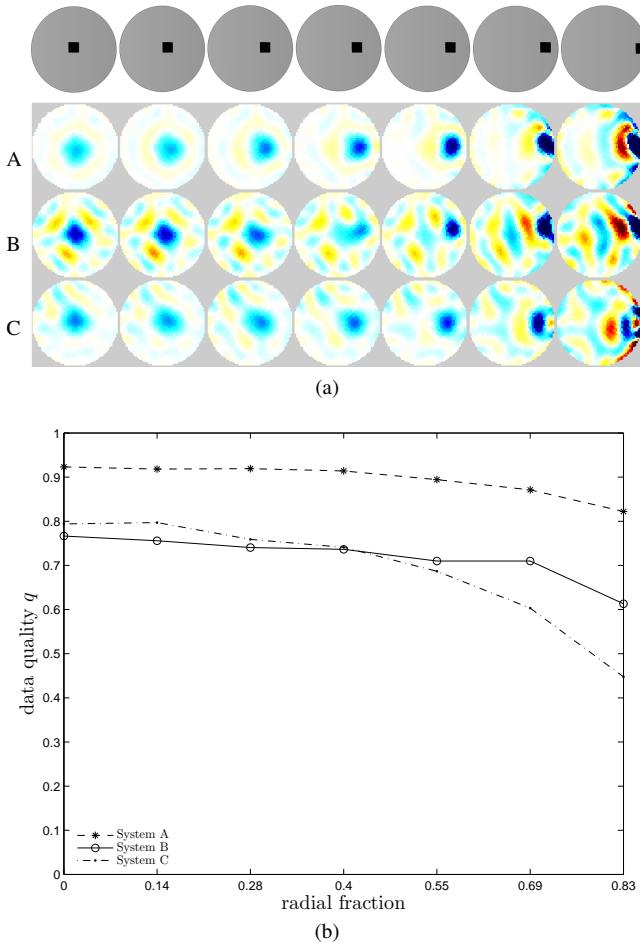


Fig. 8: Performance evaluation of EIT systems A, B and C: (a) reconstructed images of different target positions (indicated on top), and (b) the associated data quality q .

that is disturbance-free but erroneous due to incorrect setup, could also be considered a limitation in that the quality of the model affects the metric. Thus, too coarse a model or one containing meshing errors will cause q to have a lower value than would be possible with a finer model better reflecting the studied domain. However, our intention is for the quality metric to be calculated using the same forward model as the reconstructed images and to inform their interpretation. Since a poor forward model leads to poor reconstructions, we consider the dependence of the proposed quality metric q on the former to be a desirable feature.

EIT system instabilities as well as the inevitable environment noise and patient-related artifacts affect the accuracy of reconstructed EIT images and, potentially, subsequent diagnoses based on them. Due to its independence from the reconstruction algorithm and low computational cost the proposed metric is well suited for long-term real-time assessment of data quality in patients undergoing mechanical ventilation therapy, and other applications of difference EIT. When provided alongside the reconstructed images, the data quality metric can inform their analysis, preventing misinterpretations and increasing the overall reliability of the EIT technology.

APPENDIX A

FAST CALCULATION OF THE “QUALITY” MATRIX \mathbf{Q}

In this section, we develop an efficient approach to calculate matrix \mathbf{Q} . This is not critical, since the matrix is precalculated, but it is useful for equipment startup. Consider $\mathbf{Q}_i = \theta_i^T (\mathbf{I} - \mathbf{J}\mathbf{R}_i)$ and

$$\begin{aligned} \mathbf{I} - \mathbf{J}\mathbf{R}_i &= \mathbf{I} - \mathbf{J}\Sigma_m\mathbf{J}^T(\mathbf{J}\Sigma_m\mathbf{J}^T + \Sigma_n)^{-1} \\ &= (\mathbf{J}\Sigma_m\mathbf{J}^T + \Sigma_n)(\mathbf{J}\Sigma_m\mathbf{J}^T + \Sigma_n)^{-1} \\ &\quad - \mathbf{J}\Sigma_m\mathbf{J}^T(\mathbf{J}\Sigma_m\mathbf{J}^T + \Sigma_n)^{-1} \\ &= \Sigma_n(\mathbf{J}\Sigma_m\mathbf{J}^T + \Sigma_n)^{-1} \end{aligned} \quad (14)$$

where Σ_m is an estimate of the prior model element covariance, while Σ_n is an estimate of the data noise covariance. Typically, we assume that data noise is equal on all channels and thus $\Sigma_n = \lambda^2\mathbf{I}$. However, reconstruction matrix \mathbf{R}_i explicitly ignores data channel i , and thus assumes that data noise on channel i is *much* larger (by an additive factor $\mu \gg 0$). Hence, $\Sigma_n = \lambda^2(\mathbf{I} + \mu\Theta_i)$.

Thus, we can re-write eq. 14 as:

$$\begin{aligned} \mathbf{I} - \mathbf{J}\mathbf{R}_i &= \Sigma_n(\mathbf{J}\Sigma_m\mathbf{J}^T + \Sigma_n)^{-1} \\ &= \Sigma_n(\mathbf{X} + \lambda^2\mu\Theta_i)^{-1} \end{aligned} \quad (15)$$

where $\mathbf{X} = \mathbf{J}\Sigma_m\mathbf{J}^T + \lambda^2\mathbf{I}$. The inverted term represents “rank-one matrix perturbation” whose inverse may be calculated as [27]

$$(\mathbf{X} + \alpha\mathbf{a}\mathbf{b}^T)^{-1} = \mathbf{X}^{-1} - \frac{\alpha\mathbf{X}^{-1}\mathbf{a}\mathbf{b}^T\mathbf{X}^{-1}}{1 + \alpha\mathbf{b}^T\mathbf{X}^{-1}\mathbf{a}} \quad (16)$$

where $\alpha = \lambda^2\mu$ and, since $\Theta_i = \theta_i\theta_i^T$, $\mathbf{a} = \mathbf{b} = \theta_i$. When $\alpha \gg 1$ the denominator tends to

$$1 + \alpha\mathbf{b}^T\mathbf{X}^{-1}\mathbf{a} \approx \alpha\theta_i^T\mathbf{X}^{-1}\theta_i = \alpha[\mathbf{X}^{-1}]_{i,i} \quad (17)$$

so the inverted term in eq. 15 becomes

$$(\mathbf{X} + \lambda^2\mu\Theta_i)^{-1} = \mathbf{X}^{-1} - \frac{(\mathbf{X}^{-1}\theta_i)(\mathbf{X}^{-1}\theta_i)^T}{[\mathbf{X}^{-1}]_{i,i}}, \quad (18)$$

which can be calculated from \mathbf{X}^{-1} without the need to perform additional matrix inverse operations, since the inverse (denominator) in the perturbation term is scalar.

ACKNOWLEDGMENTS

The authors are grateful to Mr. Greg Kiar from Carleton University for his help in making the measurements. This work was funded in part by the Swiss Commission for Technology and Innovation (CTI Medtech Project No. 12888.1 VOUCH-LS) and Swisstom AG (Landquart, Switzerland). The work of B. Grychtol was supported by a Research Fellowship from the Alexander von Humboldt Foundation.

REFERENCES

- [1] A. Adler, M. B. Amato, J. H. Arnold, R. Bayford, M. Bodenstein, S. H. Böhm, B. H. Brown, I. Frerichs, O. Stenqvist, N. Weiler, and G. K. Wolf, “Whither lung EIT: where are we, where do we want to go, and what do we need to get there?” *Physiol. Meas.*, vol. 33, pp. 679–694, 2012.
- [2] I. Bikker, S. Leonhardt, J. Bakker, and et. al., “Lung volume calculated from electrical impedance tomography in ICU patients at different PEEP levels,” *Intensive Care Med*, vol. 35, pp. 1362–1367, 2009.

- [3] S. Meeson, B. Blott, and A. Killingback, "EIT data noise evaluation in the clinical environment," *Physiol. Meas.*, vol. 17, pp. 33–38, 1996.
- [4] F. Al-Hatib, "Patient-instrument connection errors in bioelectrical impedance measurement," *Physiol. Meas.*, vol. 19, pp. 285–296, 1998.
- [5] *Proc. NIST Biometric Quality Workshop II*, Nov. 2007.
- [6] *ISO JTC1 SC37 Biometrics, ISO 29794-1 Biometric Sample Quality, Committee Draft 1*, August 10, 2007.
- [7] A. Adler, R. Youmaran, and S. Loyka, "Towards a measure of biometric feature information," *Pattern Analysis and Applications*, vol. 12, p. 261270, 2009.
- [8] F. Vialatte, J. Sole-Casals, M. Maurice, and et. al., "Improving the quality of EEG data in patients with alzheimers disease using ICA," *Proc. 15th International Conference on Neural Information Processing, ICONIP 2008*, pp. 979–986, 2008.
- [9] T. Ferree, P. Luu, G. Russell, and D. Tucker, "Scalp electrode impedance, infection risk, and EEG data quality," *Clin Neurophysiol.*, vol. 112, pp. 536–544, 2001.
- [10] Y. Asfaw and A. Adler, "Automatic detection of detached and erroneous electrodes in electrical impedance tomography," *Physiol. Meas.*, vol. 26, pp. S175–S183, 2005.
- [11] —, "Detection of unreliable measurements in multi-sensor devices," *MeMeA 2008 - IEEE Int. Workshop on Medical Measurements and Applications*, vol. Ottawa, Canada, 2008.
- [12] G. Boverman, D. Isaacson, G. Saulnier, and J. Newell, "Methods for compensating for variable electrode contact in EIT," *IEEE Trans. Biomed. Eng.*, vol. 56, pp. 2762–2772, 2005.
- [13] E. Demidenko, "An analytic solution to the homogeneous eit problem on the 2d disk and its application to estimation of electrode contact impedances," *Physiol. Meas.*, no. 32, pp. 1453–1471, 2011.
- [14] E. Demidenko, A. Borsic, Y. Wan, R. J. Halter, and A. Hartov, "Statistical estimation of eit electrode contact impedance using a magic toeplitz matrix," *IEEE Trans. Biomed. Eng.*, vol. 58, pp. 2194–2201, 2011.
- [15] A. Hartinger, R. Guardo, A. Adler, and H. Gagnon, "Real-time management of faulty electrodes in electrical impedance tomography," *IEEE Trans. Biomed. Eng.*, vol. 56, pp. 369–377, 2009.
- [16] A. Adler, P. Gaggero, and Y. Maimaitijiang, "Adjacent stimulation and measurement patterns considered harmful," *Physiol. Meas.*, vol. 32, pp. 731–744, 2011.
- [17] P. Riu and D. Anton, "Performance assessment of EIT measurement systems," *Journal of Physics Conference Series*, vol. 224, pp. 012–015, 2010.
- [18] Y. Mamatjan, S. Böhm, P. Gaggero, and A. Adler, "Evaluation of EIT system performance," *Physiol. Meas.*, vol. 32, pp. 851–865, 2011.
- [19] A. Adler and et al, "GREIT: a unified approach to 2D linear EIT reconstruction of lung images," *Physiol. Meas.*, vol. 30, pp. S35–S55, 2009.
- [20] A. Adler and R. Guardo, "Electrical impedance tomography: regularised imaging and contrast detection," *IEEE Trans. Med. Imaging*, vol. 15, pp. 170–179, 1996.
- [21] B. Efron, "The jackknife, the bootstrap and other resampling plans," *SIAM*, vol. 38, pp. 49–59, 1982.
- [22] B. M. Graham and A. Adler, "Objective selection of hyperparameter for EIT," *Physiological measurement*, vol. 27, no. 5, pp. S65–79, May 2006. [Online]. Available: <http://www.ncbi.nlm.nih.gov/pubmed/16636421>
- [23] A. Adler, "Accounting for erroneous electrode data in electrical impedance tomography," *Physiological Measurement*, vol. 25, no. 1, pp. 227–238, Feb. 2004.
- [24] A. Adler and W. Lionheart, "Uses and abuses of EIDORS: An extensible software base for EIT," *Physiol Meas*, vol. 27, p. 25, 2006.
- [25] C. Gómez-Laberge, J. H. Arnold, and G. Wolf, "A unified approach for EIT imaging of regional overdistension and atelectasis in acute lung injury," *IEEE Trans. Med. Imag.*, no. 31, pp. 834–842, 2012.
- [26] B. Grychtol, W. Lionheart, G. Wolf, M. Bodenstern, and A. Adler, "Impact of model shape mismatch on reconstruction quality in electrical impedance tomography," *IEEE Trans. Med. Imag.*, vol. 31, no. 9, pp. 1754–1760, May 2012.
- [27] C. Gómez-Laberge and A. Adler, "Direct EIT jacobian calculations for conductivity change and electrode movement," *Physiol. Meas.*, vol. 29, pp. 89–99, 2008.